

Microinstability and Zonal-Flow Response in Mixture Plasmas with Medium-Z and Nonthermal Impurity

Motoki NAKATA^{1,2,3)}

¹⁾National Institute for Fusion Science, National Institutes of Natural Sciences, Toki 509-5292, Japan

²⁾The Graduate University for Advanced Studies, Toki 509-5292, Japan

³⁾PRESTO, Japan Science and Technology Agency, 418 Honcho, Kawaguchishi, Saitama 332-0012, Japan

(Received 19 April 2022 / Accepted 9 May 2022)

Ion- and electron-scale microinstabilities and the linear zonal-flow response in mixture plasmas with the medium-Z impurity and He-ash are investigated by means of a multi-species gyrokinetic model. In addition to the charge and dilution effects, stabilization/destabilization by nonthermal He-ash ions is clarified.

© 2022 The Japan Society of Plasma Science and Nuclear Fusion Research

Keywords: burning plasma, He-ash, impurity, microinstability, zonal flow, gyrokinetic simulation

DOI: 10.1585/pfr.17.1203078

In contrast to experimental plasmas to usually maximize the hydrogen/deuterium purity, burning plasmas are intrinsically mixture states with multiple ion species. In several experiments, the suppression of confinement degradation has been observed in the impurity-seeded plasma [1, 2]. Moreover, the medium-Z impurity seeding in the core and edge regions is considered to be necessary for achieving a sufficient radiation loss in DEMO reactors [3]. In such mixture plasmas, ion- and electron-scale microinstabilities, the associated turbulent transport, and zonal-flow generation are influenced by right and/or heavy impurities, and by thermal and/or nonthermal He-ash ions, as well as the fuel isotope ions [4]. The ion-scale instabilities have mainly been addressed in earlier works [5–8].

In this study, the impacts of medium-Z impurity and He-ash ions on both the ion-temperature-gradient (ITG) and electron-temperature-gradient (ETG) instabilities are investigated by means of a multi-species gyrokinetic model and the numerical simulations. Particular focus is put on the dilution and the unequal temperature for the ion species. The linear zonal-flow response is also examined.

Here, dispersion equations for the ITG and ETG modes in mixture plasmas are derived. The linearized electrostatic gyrokinetic equation for the species “s” and the Poisson equation are given by

$$\mathcal{L}_s \delta g_{sk_\perp} = (\omega - \omega_{*T_s}) \frac{e_s \delta \phi_{k_\perp}}{T_s} J_0(k_\perp^2 \rho_{ts}^2) F_{Ms}, \quad (1)$$

$$(k_\perp^2 + \lambda_D^{-2}) \delta \phi_{k_\perp} = 4\pi \sum_s e_s \int dv J_0(k_\perp^2 \rho_{ts}^2) \delta g_{sk_\perp}, \quad (2)$$

where the collisionless limit in the Fourier-Laplace form is considered, and $\mathcal{L}_s := \omega - k_\parallel v_\parallel - \omega_{Ds}$ with the complex frequency ω . The non-adiabatic distribution function and

the potential fluctuation are denoted by δg_{sk_\perp} and $\delta \phi_{k_\perp}$, respectively. The squared inverse of the Debye length is given by $\lambda_D^{-2} := \sum_s \lambda_{Ds}^{-2}$ with $\lambda_{Ds}^{-2} = 4\pi n_s e_s^2 / T_s$. The thermal gyroradius ρ_{ts} is defined by $\rho_{ts} = m_s v_{ts} / e_s B_{ax}$ with the thermal speed of $v_{ts} = (T_s / m_s)^{1/2}$. More details are presented in e.g., Refs. [9] and [10].

In this paper we treat 3 or 4 ion species: $s = \{e, H(=i), He, Ar\}$. Then, the dispersion equation for the ITG mode is derived by combining Eqs. (1) and (2) in the long-wavelength approximation ($k_\perp^{-1} > \rho_{He} \geq \rho_H > \rho_{Ar} > \rho_e$),

$$k_\perp^2 + \lambda_D^{-2} = \sum_{s \neq e} \lambda_{Ds}^{-2} \int dv \mathcal{L}_s^{-1} (\omega - \omega_{*T_s}) J_0^2(k_\perp^2 \rho_{ts}^2) F_{Ms}, \quad (3)$$

where the electrons are assumed to be adiabatic, i.e., $\delta g_{ek_\perp} = 0$. Further reductions in the fluid limit $k_\parallel v_\parallel / \omega \ll 1$, $\omega_{Ds} / \omega \ll 1$, and $\omega_{*T_s} / \omega \ll 1$ yield

$$\omega^2 = \frac{-\omega_{*T_i} \omega_{Di} \sum_{s \neq e} f_{Cs} Z_s^{-1} (T_s / T_i) \Gamma_{0s} \left(\frac{L_{ns}^{-1} + L_{Ts}^{-1}}{L_{ni}^{-1} + L_{Ti}^{-1}} \right)}{k_\perp^2 \lambda_{Die}^2 + (T_i / T_e) + \sum_{s \neq e} f_{Cs} Z_s (T_s / T_i)^{-1} (1 - \Gamma_{0s})}, \quad (4)$$

where $\lambda_{Die}^2 := T_i / 4\pi n_e e^2$ and $\Gamma_{0s} := I_0(k_\perp^2 \rho_{ts}^2) \exp(-k_\perp^2 \rho_{ts}^2)$ with the modified Bessel function I_0 describe the finite Debye length and the finite gyroradius effects, respectively. The charge number and the charge density fraction are represented by Z_s and $f_{Cs} := n_s Z_s / n_e$, where $\sum_s f_{Cs} = 1$. The velocity dependence in ω_{*T_s} and ω_{Ds} is ignored for simplicity, by evaluating $v^2 \sim 4T_s / m_s$. The impurity and nonthermal ion effects also appear in $k_\perp^2 \rho_{ts}^2 = k_\perp^2 \rho_s^2 A_s (T_s / T_i) Z_s^{-2}$

As for the ETG mode, one can derive the dispersion equation in the long-wavelength approximation ($\rho_{He} \geq \rho_H > \rho_{Ar} > k_\perp^{-1} > \rho_e$),

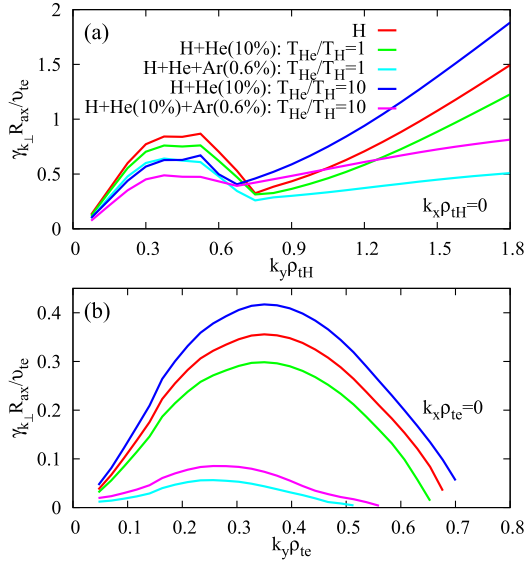


Fig. 1 Growth rate of (a) ITG and (b) ETG modes.

$$\omega^2 = \frac{-\omega_* T_e \omega_{De} \Gamma_{0e}}{k_{\perp}^2 \lambda_{De}^2 + 1 - \Gamma_{0e} + (T_e/T_i) \sum_{s \neq e} f_{Cs} Z_s (T_s/T_i)^{-1}}, \quad (5)$$

where all ion species is adiabatic due to $J_0(k_{\perp}^2 \rho_{ts \neq e}^2) \rightarrow 0$. For both Eqs. (4) and (5), the charge and dilution effects are incorporated in the dispersion equation. Note also that the unequal temperature for ions is explicitly treated in order to examine the impact of the nonthermal He-ash ions.

In the dispersion equations, one can see the qualitative impacts of the impurity (Ar) and nonthermal He-ash ions. The dilution effect to the main hydrogen ions in the presence of impurity leads to the stabilization of the ITG mode, as seen in $f_{Cs} Z_s^{-1}$ of Eq. (4). One also finds that the ETG mode growth rate is reduced by the effective charge, which is represented by $\sum_{s \neq e} f_{Cs} Z_s = Z_{eff}$ in Eq. (5).

On the other hand, nonthermal He-ash ions cause the opposite impact. Although He-ash ions have the low- Z charge and the similar gyroradius to the main hydrogen ions in the thermalized state, the ITG and ETG modes are affected by unthermalized hot He-ash ions with $T_{He}/T_H > 1$. The destabilization of the ETG mode is easily found from $(T_s/T_i)^{-1}$ in Eq. (5), whereas the complicated dependence appears in the ITG case of Eq. (4) with Γ_{0s} .

In order to examine the above theoretical arguments, the gyrokinetic Vlasov simulations with GKV [11] have been carried out for the mixture plasma of the Hydrogen, Helium, Argon ions, and the kinetic electrons. Here, both the ITG and ETG modes are solved in a fluxtube of the axisymmetric configuration, and $R/L_{ns} = 2$, $R/L_{Ts} = 8$ for all species. Inspired from the ITER and DEMO [3], $n_{He}/n_e \sim 10\%$ and $n_{Ar}/n_e \sim 0.6\%$ are considered.

Figures 1 (a) and 1 (b) show the poloidal wavenumber spectra of the ITG and ETG mode growth rate, respectively. As is theoretically expected, the dilution effects by He and

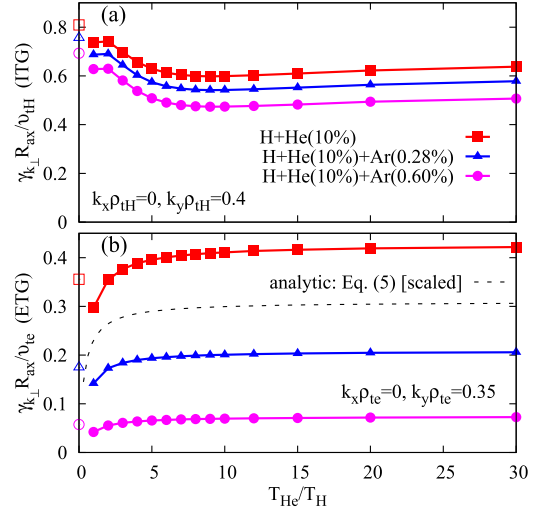
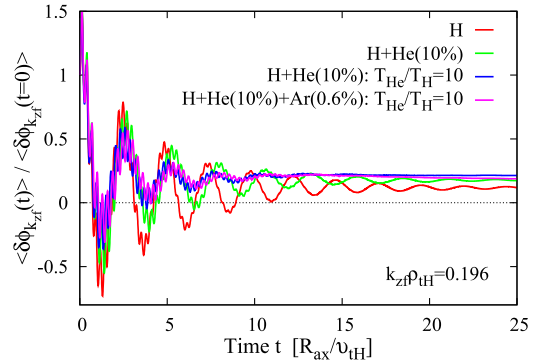

 Fig. 2 T_{He}/T_H dependence of (a) ITG and (b) ETG growth rate. The open symbols are the cases without He. The analytic evaluation is applied for the case of H+He(10%).


Fig. 3 Linear zonal-flow response.

Ar ions lead to the stabilization for both. Particularly, a significant stabilization of the ETG mode appears for the case with Ar impurity. One also finds that the nonthermal He-ash ions with $T_{He}/T_H = 10$ reduces the ITG mode growth rate, while the ETG mode becomes more unstable. Then the ratio of the ETG growth rate to the ITG growth rate, i.e., $r_{\gamma} := \gamma_{k_{\perp}}(k_y \rho_{te} = 0.35) / \gamma_{k_{\perp}}(k_y \rho_{tH} = 0.45)$, is enlarged by hot He-ash ions, where r_{γ} in the case of H+He(10%) with $T_{He}/T_H = 10$ is 1.65 times larger than that in the case with $T_{He}/T_H = 1$.

The opposite impacts of T_{He}/T_H in the ITG and ETG modes are demonstrated in Figs. 2 (a) and 2 (b). One finds the nonlinear and/or nonmonotonic dependence for both cases in $1 \leq T_{He}/T_H \leq 15$. Note that the analytic evaluation by Eq. (5) for the case of H+He(10%) qualitatively reproduces the numerical result.

Lastly the linear zonal-flow responses are compared in Fig. 3. It is found that both the dilution and nonthermal effects by He-ash lead to less GAM damping with enhanced residual zonal-flow level. The enhanced residuals can be

attributed from the decrease of shielding effect to the zonal potential, depending on the radial drift excursion of trapped ions with different gyroradius and the density fraction.

Also, one can see that the residual level does not change so largely, but gradually decreases in time for the case of H+He(10%)+Ar(0.6%) with $T_{\text{He}}/T_{\text{H}} = 10$, compared to the case without Ar. Such a weak impact of the Ar ions is associated with relatively smaller radial drift of the minority Ar ions [$\propto \rho_{\text{Ar}} = \rho_{\text{H}}/(Z_{\text{Ar}}/2)^{1/2} = \rho_{\text{H}}/3$] in comparison to those of the bulk H ions. Then the shielding to the zonal potential by the Ar drift motion becomes less effective. On the other hand, the increased collisionality by Ar enhances the collisional zonal-flow damping. Nonlinear zonal-flow dynamics and its impact on the turbulent transport will be addressed in future work.

This work is supported by JST, PRESTO Grant Number JPMJPR21O7, in part by the NIFS collaborative

Research Programs (NIFS22KIST017, NIFS22KIST018), and in part by PLADyS, JSPS Core-to-Core Program. Numerical simulations were performed by JFRS-1 at IFERC-CSC, and Plasma Simulator at NIFS.

- [1] M.N.A. Beurskens *et al.*, Plasma Phys. Control. Fusion **55**, 124043 (2013).
- [2] H. Urano *et al.*, Nucl. Fusion **55**, 033010 (2015).
- [3] N. Asakura *et al.*, Nucl. Fusion **61**, 126057 (2021).
- [4] M. Nakata *et al.*, Phys. Rev. Lett. **118**, 165002 (2017).
- [5] C. Estrada-Mila *et al.*, Phys. Plasmas **13**, 112303 (2006).
- [6] C. Angioni *et al.*, Phys. Plasmas **15**, 052307 (2008).
- [7] T. Dannert *et al.*, Phys. Plasmas **15**, 062508 (2008).
- [8] S.M. Yang *et al.*, Phys. Plasmas **25**, 122305 (2018).
- [9] M. Nakata *et al.*, Plasma Fusion Res. **9**, 1403029 (2014).
- [10] M. Nakata *et al.*, Nucl. Fusion **56**, 086010 (2016).
- [11] T.-H. Watanabe *et al.*, Nucl. Fusion **46**, 24 (2006).